

Article

β -Phase-Induced Quasi-Cleavage Fracture Mechanism by Dual-Phase High-Strength Titanium Alloy at Elevated Temperature

Wenlan Wei , Hao Qu, Jiarui Cheng * , Rui Zhang, Yinping Cao  and Lu Cui 

Xi'an Key Laboratory of Wellbore Integrity Evaluation, Xi'an Shiyou University, Xi'an 710065, China

* Correspondence: cjr88112@163.com

Abstract: Dual-phase high-strength titanium alloy has the properties of high specific strength and good toughness, which have resulted in its gradual use in the fields of oil and gas well engineering. The elevated-temperature service environment of deep strata is its key research direction. In this paper, the strength and fracture mechanism of a new type of $\alpha + \beta$ -phase titanium alloy tubing material in its service-temperature range are studied. Its fracture mechanism changed at 130 °C to 150 °C, from normal-stress ductile fracture to quasi-cleavage fracture formed by β -phase voids, which induced microshear, which significantly reduced the elongation of the material and accelerated the rate of yield strength decline with temperature. This mechanism provides a new guiding idea for the design of the microstructure and element content of dual-phase high-strength titanium alloy. For titanium alloy materials in service within the temperature range of the fracture mechanism transition, which is between 130 °C and 150 °C, reducing the void-inducing factors in the β -phase or reducing the content of the β -phase to avoid microshear failure should be considered.

Keywords: titanium alloy; fracture mechanism; strength; high-temperature tensile; tubing



Citation: Wei, W.; Qu, H.; Cheng, J.; Zhang, R.; Cao, Y.; Cui, L.

β -Phase-Induced Quasi-Cleavage Fracture Mechanism by Dual-Phase High-Strength Titanium Alloy at Elevated Temperature. *Crystals* **2022**, *12*, 1255. <https://doi.org/10.3390/cryst12091255>

Academic Editor: Cyril Cayron

Received: 12 August 2022

Accepted: 2 September 2022

Published: 5 September 2022

Publisher's Note: MDPI stays neutral with regard to jurisdictional claims in published maps and institutional affiliations.



Copyright: © 2022 by the authors. Licensee MDPI, Basel, Switzerland. This article is an open access article distributed under the terms and conditions of the Creative Commons Attribution (CC BY) license (<https://creativecommons.org/licenses/by/4.0/>).

1. Introduction

In recent years, titanium alloy materials with high-specific-strength properties have been used in drill pipes, tubing, casing and other pipe strings used in petroleum engineering [1–3]. Its light and high-strength properties make it possible to work in deep and ultra-deep wells. The load caused by gravity is far less than that of steel, which gives titanium alloy pipe strings a wide application prospect in the field of petroleum engineering. For the material selection of titanium alloy oil pipes, high-strength titanium alloy materials with a yield strength greater than 700 MPa are usually used, especially for oil wells with a depth of more than 3000 m. Moreover, the formation temperature of deep wells is also significantly higher than that of ordinary oil wells—that is, more than 150 °C—and its high-temperature strength is key to its performance of service safety [4,5].

For titanium alloy oil pipes, their properties should not only meet the requirements of strength and toughness but also meet the anticorrosion requirements under Cl⁻, H₂S, CO₂ and other corrosive conditions [6–9]. Generally, α -phase titanium alloys are mainly solution-strengthened by adding Al, Mo, V and other alloy elements, so as to obtain a near- α -phase structure [10]. Although solution strengthening significantly improves the strength of titanium alloy, the strength of α -phase titanium alloy is still lower than that of ordinary steel for oil pipe strings because it cannot be strengthened by heat treatment, which makes it difficult to meet the actual use needs [11,12]. The microstructure of β -phase titanium alloys is usually a metastable β -phase, and only the β -phase is contained after air cooling above its transition temperature. These kinds of titanium alloys usually have high strength and poor stability and toughness [13–15]. After aging treatment, the metastable β -phase titanium alloy precipitates a small granular α -phase structure in its metastable grains, so as to obtain better toughness and higher strength [16]. Then, the strength and

plasticity of the β -phase titanium alloy are determined by the distribution and grain size of the α -phase. The smaller the grain size of the α -phase, the higher the strength of the titanium alloy [17–19].

For titanium alloy materials used in the field of petroleum engineering, a dual-phase titanium alloy composed of α -phase (HCP structure) and β -phase (BCC structure) is mostly used. It mainly includes Ti-6Al-4V [20], Ti-6Al-2Sn-4Zr-6Mo [21], Ti-6Al-4VRu [22], etc. The research [23–25] presents that the higher the temperature of the dual-phase coexistence temperature range during the heat treatment of $\alpha + \beta$ -phase dual-phase titanium alloy, the more the α -phase structure is transformed from the β -phase in the subsequent cooling process. In addition to the solid solution-strengthening effect, the strength of duplex titanium alloy can be further improved by the precipitation of the α -phase from the β -phase during aging treatment [26]. For titanium alloys with Mo content less than 10%, such as Ti-6246, the equiaxed microstructure transformed from the β -phase after dynamic recrystallization and heat treatment has a yield strength of more than 950 MPa, and has high performance in plasticity and fracture toughness. The fracture process presents uniform ductile fractures [27,28]. Relevant research shows that the yield strength is still above 760 MPa at temperatures above 200 °C [29]. In previous studies [30,31], the dual-phase titanium alloy containing Mo and Cr showed high strength and good toughness after grain refinement and quenching and tempering. However, these studies focused on room temperature.

Research on the high-temperature strength of duplex titanium alloys is mostly focused on above 400 °C [32,33], while research on the mechanical behavior and service safety at 70–220 °C concerning the field of petroleum engineering is less. In this study, a new 110 ksi dual-phase titanium alloy tubing material with good toughness and a new design is selected, which meets the service strength requirements. Its main alloy elements are Al, Zr, Mo and Cr. The mechanical behavior in its service temperature range showed a new ductile quasi-cleavage mixed-fracture mechanism different from that at above 500 °C. Then, the discovery of the microshear mechanism of the β -phase makes it possible for the microstructure to avoid the risk of service failure in the process of material design, and its fracture mechanism is the main work of this study.

2. Materials and Experimental Methods

2.1. Materials and Microstructure

The material selected in this study is Al-Mo-Cr-Zr dual-phase titanium alloy. High temperature tensile test and fracture mechanism characterization analysis are carried out. The element composition is shown in Table 1. The main structure of the material is granular structure $\alpha + \beta$ -phase, in which α -phase accounts for 48.4%, β -phase accounts for 51.6% and the microstructure is shown in Figure 1. The grains of α - and β -phase are evenly distributed, and their average grain diameter is less than 10 μm . A few β -phase grains of diameter greater than 15 μm , second-phase particles and inclusions are difficult to observe.

Table 1. Chemical compositions (wt.%).

Ti	Cr	Mo	Zr	Al	Fe	C
88.3	3.3	3.5	0.6	4.3	0.02	0.03

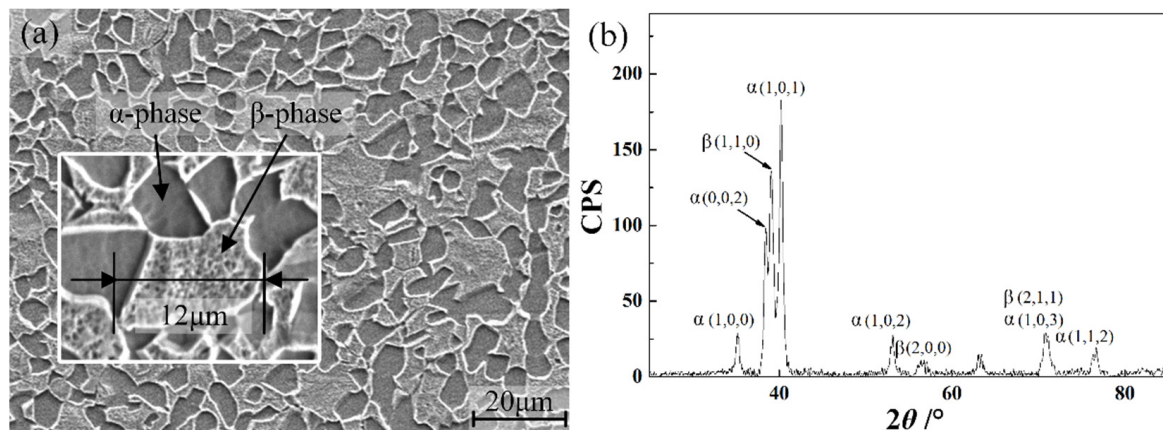


Figure 1. Microstructure of dual-phase titanium alloy: (a) SEM; (b) XRD.

2.2. Experimental Method

According to ISO 6892-2-2018 (metallic materials—tensile testing), round-bar tensile specimens are selected for high-temperature tensile test. The tensile specimen is cut directly from the oil pipe. The diameter of the specimen is 5 mm and the gauge distance is 35 mm, as shown in Figure 2. According to the actual service temperature of the tubing, the temperature of the tensile test increases from room temperature (20 °C), increasing to 100 °C every 20 °C, and then increasing to 200 °C every 10 °C. The tensile tests were conducted using servohydraulic testing machine (Instron 8862). The loading rate of tensile test is 1 mm / min and the test temperature is controlled by the resistance furnace (the temperature error is ± 1 °C). After reaching the test temperature, it is kept for 30 min and then loaded.

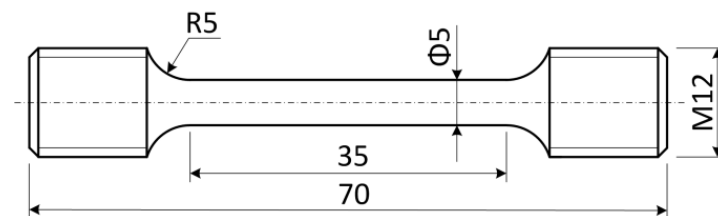


Figure 2. Dimension of tensile specimen.

The microstructure sample was sliced directly from the titanium alloy casing. After polishing the specimen, the surface was eroded by an etchant (5% HF + 10% HNO₃ + 85% H₂O) to obtain a surface with observable microstructure morphology. The microstructure morphologies were obtained by scanning electron microscope (TESCAN VEGA2). The line-scanning method is used for EDS analysis to make it pass through multiple α + β -phase grains, so as to obtain the element segregation comparison results of different phases. The fracture surface of tensile sample after ultrasonic cleaning was observed by scanning electron microscope. Then, the macrofracture morphology and the characteristics of fracture source area were photographed, respectively.

3. Results

3.1. Tensile Strength Affected by Temperature

In the range of room temperature (20 °C) to 200 °C, the tensile curves of Al-Zr-Mo-Cr titanium alloy are shown in Figure 3, respectively. There is no obvious yield platform in the tensile curve. At 20–150 °C, it presents a smooth curve from elastic stage to plastic stage. At 200 °C, there is an obvious yield point after the elastic stage, and the yield platform does not appear. Due to the increase in temperature, the strength of the material shows a downward trend, The increase in temperature usually increases the elongation of the tensile test for plastic materials. It is worth noting that the test results of Al-Zr-Mo-Cr

titanium alloy show abnormal characteristics. Then, the elongation of the material in the tensile results at 150 °C is significantly lower than that at 100 °C.

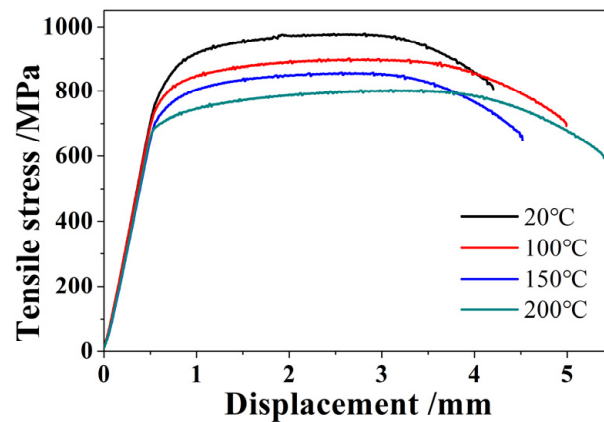


Figure 3. Engineering stress–displacement curve of Al-Zr-Mo-Cr titanium alloy.

The tensile test results with smaller test temperature steps are shown in Figure 4. In the temperature range from 20 °C to 200 °C, the yield strength of the material shows obvious bilinearity (Figure 4a). When the temperature is lower than 140 °C, the yield strength decreases linearly with temperature, while when the temperature is higher than 140 °C, the declining trend of yield strength with temperature is obviously accelerated. The relationship between elongation and test temperature is shown in Figure 4b. The elongation of the material increases with the increase in temperature when the temperature is lower than 140 °C. It is worth noting that at 140 °C, the elongation decreases suddenly and significantly, and then increases continuously with the increase in temperature. Obviously, in the range of 130–150 °C, the fracture mechanism of the material changes, resulting in a significant change in elongation.

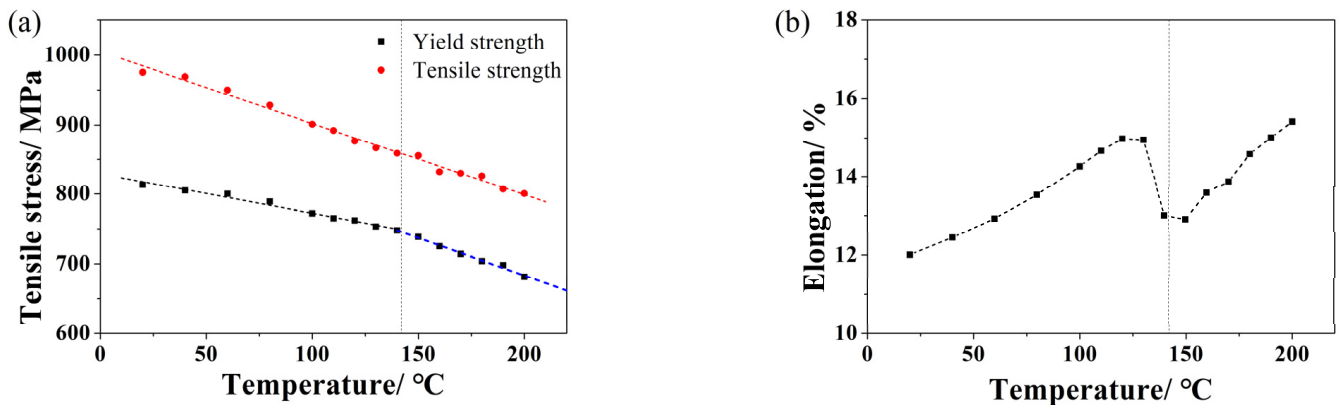


Figure 4. Effect of temperature on mechanical properties: (a) yield strength and tensile strength; (b) elongation.

3.2. Fracture Analysis

At different temperatures, the tensile fracture of Al-Zr-Mo-Cr titanium alloy is composed of a fiber source region and a shear lip region (Figure 5a–d). There is an obvious boundary between the macrocharacteristics of the two regions. Then, the fracture process of the material consists of the microvoids generated in the material gradually increasing with the progress of tension, and the micropores polymerizing in the fiber area to form normal stress, resulting in the slow propagation of the crack in the source area. Necking causes the load at the crack tip to change from normal stress to shear stress, which makes the crack in the source region expand rapidly and stably and forms a shear lip region.

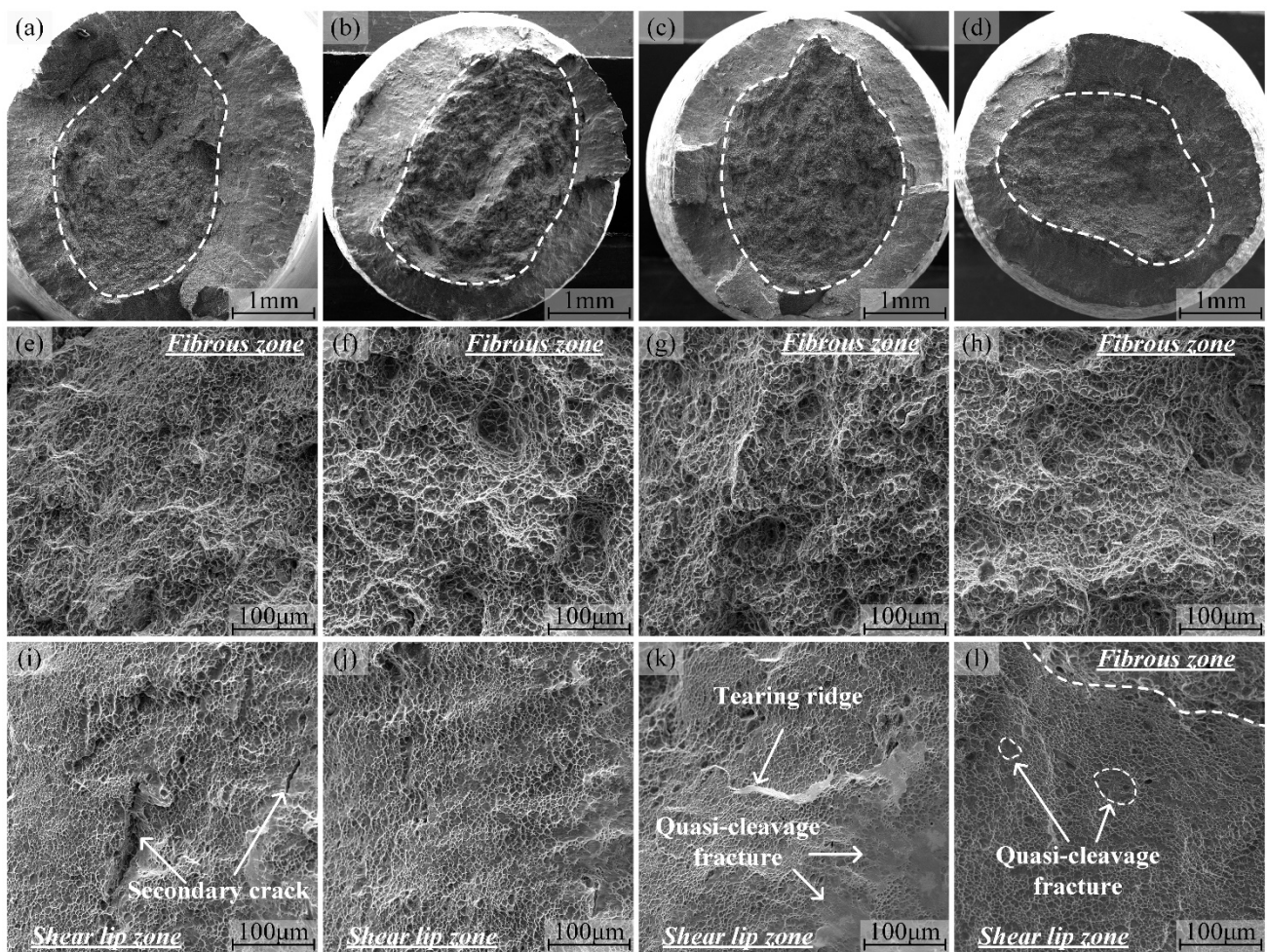


Figure 5. Fracture morphology: (a) 20 °C, (b) 100 °C, (c) 150 °C, (d) 200 °C; fibrous zone: (e) 20 °C, (f) 100 °C, (g) 150 °C, (h) 200 °C; shear lip zone: (i) 20 °C, (j) 100 °C, (k) 150 °C, (l) 200 °C.

The radiation region is not observed between the fiber region and the shear lip region, which indicates that there is no transition from stable crack growth to rapid unstable crack growth, and the crack growth rate increases suddenly from the fiber source region to the shear lip region. The fracture characteristics of the fiber source region under different temperature conditions are shown in Figure 5e–h. The fiber source region presents ductile fracture characteristics, which is a typical microvoid polymerization fracture. The increase in temperature has no obvious effect on the ductile fracture process, and the diameter of the dimple of all fractures is 8–15 μm for different temperature conditions.

The influence of different temperatures on the fracture morphology of the material is mainly manifested in the shear lip region. At room temperature (20 °C), the shear lip region is still characterized by the dimple (Figure 5i). It is different from the fiber source region. The dimple has obvious directionality and presents the characteristics of a semi-open dimple in the direction of crack propagation. There are also a large number of secondary cracks in the shear lip region, whose direction is perpendicular to the crack propagation direction, and the length is 40–130 μm. With the increase in temperature, the number of secondary cracks decreases significantly when the test temperature is 100 °C (Figure 5j), and the secondary crack initiation characteristics with small length (<60 μm) and shallow depth can be observed. When the test temperature is 150 °C (Figure 5k), no secondary crack is observed in the whole shear lip area, and the dimple shape is different from that at lower temperature. The deep void accumulates in some parts of the shear lip, usually near the tear ridge. Moreover, there are a large number of smooth quasi-cleavage fracture characteristics in the whole semi-open dimple region. When the temperature reaches 200 °C (Figure 5l), a

large number of quasi-cleavage features with small area are associated around the void in the shear lip area.

Obviously, the change in the fracture process in the shear lip region is caused by the increase in temperature. At room temperature (20 °C), due to the influence of shear stress, the void defects in the material occur stress concentration perpendicular to the crack growth direction, resulting in the formation of secondary cracks perpendicular to the crack growth direction in the void.

With the increase in temperature, the activation energy inside the material increases, and the energy level required for the atomic slip is lower. When the concentrated stress around the cavity is insufficient to provide effective fracture energy for the material, the slip occurs. Therefore, the characteristics of secondary cracks gradually disappear with the increase in temperature. The concentrated stress around the void is not enough to provide sufficient activation energy for microcrack propagation, that is, a slip is formed. Thus, the characteristics of secondary cracks gradually disappear with the increase in temperature. At a higher temperature (150 °C), there are more—and aggregated—voids in the shear lip region, which indicates that the formation mechanism of voids changes due to the influence of temperature before the occurrence of cracks. In addition, the quasi-cleavage features at this temperature show that the normal stress of local microstructure increases significantly, which induces the formation of quasi-cleavage fracture. With the further increase in temperature, the increase in activation energy also reduces the concentration stress at the void accumulation location, resulting in a reduction in the quasi-cleavage surface area and the formation of a large number of quasi-cleavage features. The fracture analysis shows that with the temperature increase, the fracture crack propagation process in the shear lip region gradually changes from the ductile fracture to the mixed-fracture form of quasi-cleavage and ductile fracture, and the occurrence of aggregated voids in the shear lip region is an important factor causing the change in fracture mechanism.

Void damage is the main cause of stress concentration in the local area of the microstructure. At 20 °C, the microstructure of the fracture section is shown in Figure 6a, and all voids are formed in the α -phase, and microcracks first form from the cavity position of the α -phase and gradually expand to form dimple characteristics. When the temperature is 100 °C, transcrystalline microcracks formed by voids in the adjacent α -phase are observed, and the position of voids is still present in the α -phase. Then, the voids in the β -phase of the fracture section are observed when the temperature increases to 150 °C. It can be inferred that the cracking characteristics of the β -phase change when the temperature increases, and it is easier to form voids. Under this condition, α -phase and β -phase voids appearing in both phases, which reduce the statistical expectation of the distance between two adjacent voids, and it is easier to cause normal-stress fracture between two short-distance voids, rather than ductile fracture. Therefore, the fracture characteristics of quasi cleavage fracture are formed. When the temperature is further increased to 200 °C, the number of voids in the α -phase and β -phase increases significantly, which forms void aggregation, and then reduces the normal stress between adjacent short-distance voids, so the number and area of quasi-cleavage features at this temperature decrease.

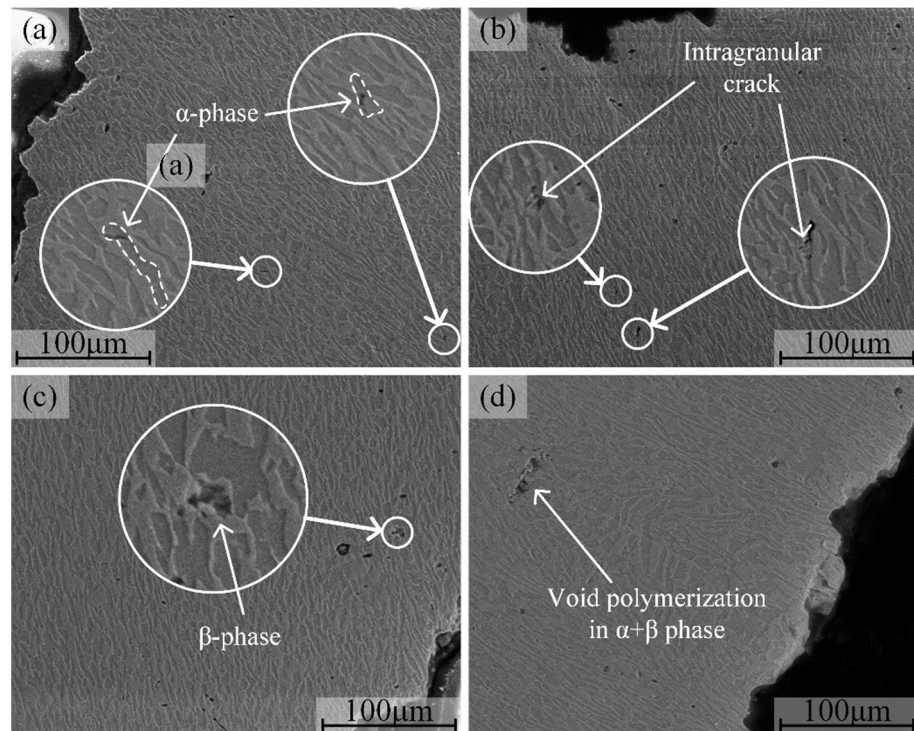


Figure 6. Tensile fracture section at different temperatures: (a) 20 °C; (b) 100 °C; (c) 150 °C; (d) 200 °C.

4. Discussion

4.1. Fracture Mechanism of Temperature Influence

The yield strength of the material decreases significantly with the change in temperature when the temperature is above 140 °C, and the voids in the α -phase and β -phase were observed in the fracture section of the test samples. Only the void in the α -phase for the fracture morphology below 140 °C is observed. The rise in temperature obviously leads to the change of the damage mechanism with the β -phase.

The material contains four main alloy elements: Al, Zr, Cr and Mo, and its microstructure is scanned by energy-dispersive spectroscopy (EDS) analysis with a line, as shown on the left side of Figure 7. The dark color and sunken part are the α -phase, the light color and prominent part are the β -phase, and the distribution results of solid-solution elements in different phases are shown on the right side of Figure 7. EDS results show that Al and Zr are evenly distributed in the α -phase and β -phase, and there is no obvious segregation; however, both Cr and Mo elements have obvious segregation in the β -phase, and the content of Cr and Mo elements in the α -phase is low.

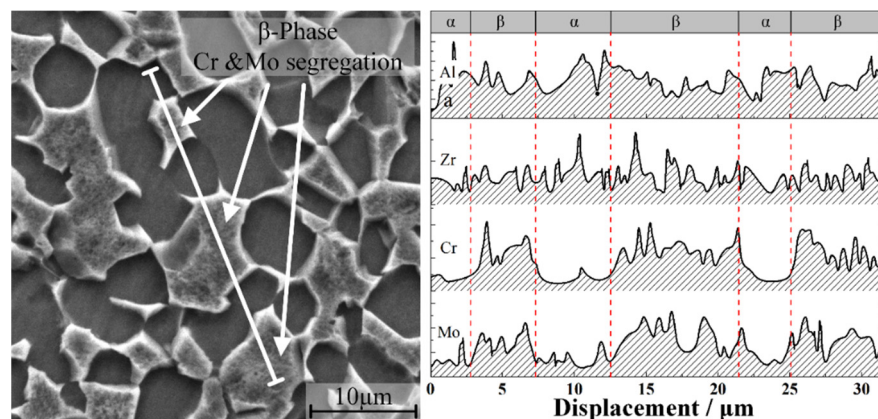


Figure 7. Segregation of Al, Mo, Cr and Zr in $\alpha + \beta$ phase.

For dual-phase titanium alloy materials, the crystal lattice structure of β -phase is BCC and the crystal lattice structure of α -phase is HCP. Compared with BCC, HCP has poor plasticity and is difficult to slip during deformation. When the dual-phase titanium alloy is subject to large deformation and there are no other influencing factors, the BCC structure, i.e., β -phase, slip occurs firstly. Then, the HCP structure with poor deformation ability, i.e., α -phase, forms void defects, which cause the stress release of the microstructure around the voids. When the deformation continues to increase, the internal voids of the β -phase are difficult to form due to the stress release. Therefore, the α -phase forms voids inside at room temperature, while the β -phase does not. Moreover, the voids in the α -phase begin to propagate as the crack source, then form ductile fracture characteristics.

With the increase in test temperature, the atomic activation energy in the grain increases, and the stress required to form a slip is reduced. Then, the segregation elements Cr and Mo in the β -phase increase their ability to resist sliding at high temperature [34,35], that is, the deformation ability of the β -phase is reduced, and the stress cannot be released effectively, which significantly improves the probability of forming voids in the β -phase. Furthermore, higher atomic activation energy increases its plasticity for the α -phase. For the joint action of these two influencing factors, when the material is deformed, voids can be formed in the β -phase while the α -phase begins to form, resulting in a significant reduction in the distance between the two voids. When the deformation further increases, the concentrated stress in the micro area between two adjacent voids increases significantly, and the conditions for the crack propagation caused by the void to form ductile fracture are gradually not satisfied, and the probability of quasi-cleavage fracture is raised by the increased normal stress. With the condition of the large shear stress component, the significantly increased normal stress causes the crack propagation mechanism to change from ductile propagation to quasi-cleavage propagation (Figure 8), which is the main reason for the formation of quasi-cleavage morphology in the shear lip region.

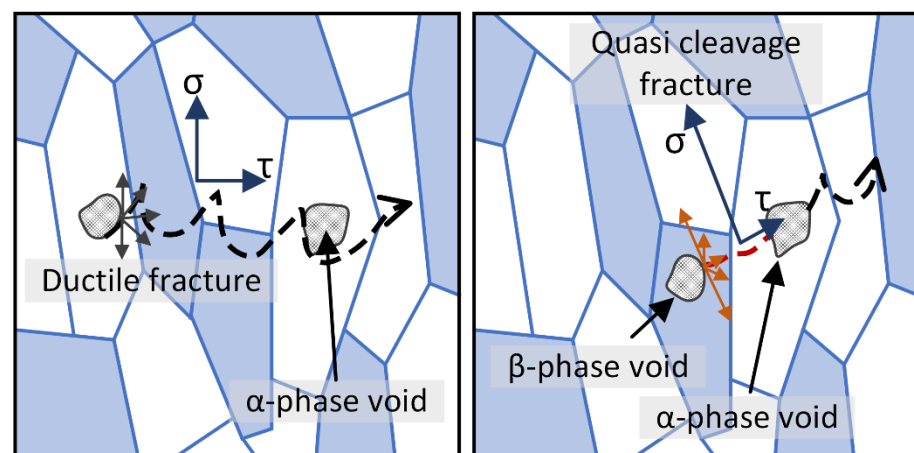


Figure 8. Temperature affects the change of fracture mechanism.

In other words, the appearance of β -phase voids is the inducement of fracture mechanism transformation. Firstly, due to the temperature increase, the void in the β -phase can be formed during deformation. Secondly, for the case where there are voids in both the α -phase and β -phase, the expected distance between voids is smaller than that in the case where only the α -phase has voids, and it is easier to achieve the conditions for inducing quasi-cleavage fracture, thus changing the fracture process.

4.2. Strength Decrease Caused by Temperature

The increased atomic activation energy is due to the rise in temperature, which makes it easier to form a slip, improves the macrodeformation ability of the material and reduces the stress required to form microzone damage, so the yield strength of this titanium alloy

in the range of room temperature to 140 °C decreases continuously with the increase in temperature, and the elongation increases with the increase in temperature.

The deformation mechanism of the β -phase is changed when the test temperature exceeds 140 °C. The segregation of Cr and Mo elements in the β -phase causes the stress concentration in the microregion of the grain, so it forms a void damage that is not found at room temperature in the β -phase, resulting in a decline in bearing capacity. Therefore, when the temperature exceeds 140 °C, the rate of yield strength decreasing with temperature is higher than that below 140 °C. Moreover, due to the joint influence of the α -phase and β -phase voids, the ductile propagation process of crack changes to the fracture process of partial quasi-cleavage propagation below 140 °C, which reduces the ductility and increases the brittleness of the material macroscopically, resulting in a significant reduction in its elongation. When the temperature is further increased, the quasi-cleavage fracture mechanism is affected by the increasing atomic activation energy, and the deformation ability of the material increases again with the elevated temperature; that is, the elongation continues to increase.

The fracture mechanism of the β -phase is determined by two factors: one is the atomic activation energy, and the other is the strengthening characteristics of Cr and Mo on the β -phase at high temperature. When the material yields and voids are formed in the β -phase, the voids reduce its strength, while the β -phase without void damage continues to be strengthened by Cr and Mo atoms, resulting in the further improvement in residual β -phase strength. The two mechanisms jointly determine the macrostrength of the material. It can be inferred from the change trend of the tensile strength with temperature that the effects caused by these two mechanisms almost offset each other, and the decrease in macrostrength is mainly affected by atomic activation energy.

5. Conclusions

In this paper, the mechanism of the accelerated strength decline of Al-Zr-Mo-Cr dual-phase titanium alloy caused by elevated temperature was studied. The results show that the tensile fracture mechanism of the dual-phase titanium alloy gradually changed from a ductile fracture at room temperature to a mixed-fracture form of ductile fracture and quasi-cleavage fracture at the temperature range between room temperature and 200 °C, instead of the generally considered ductile fracture. Moreover, it led to the increase in the yield-strength decreasing rate with the increase in temperature and the abnormal change of elongation, when the ambient temperature exceeded 140 °C. The reason for the fracture mechanism transformation is that the segregation of Cr and Mo elements in the β -phase at high temperature caused the void initiation in the β -phase, and the crack propagation mode changed from ductile to quasi-cleavage. The phenomenon of quasi-cleavage fracture induced by voids in the β -phase deserves continuous attention. In the future, we will use the molecular dynamics method to further explore the law of this phenomenon and the critical parameters of quasi-cleavage induced.

Author Contributions: Conceptualization, W.W.; methodology, Y.C. and L.C.; validation, R.Z.; investigation, H.Q.; writing—original draft preparation, W.W.; writing—review and editing, W.W.; project administration, J.C.; funding acquisition, W.W. All authors have read and agreed to the published version of the manuscript.

Funding: This research was funded by the National Natural Science Foundation of China grant number 51901180, Scientific Research Program Funded by Shaanxi Provincial Education Department grant number 21JP096 and Natural Science Foundation of Shaanxi Province of China grant number 2020JM538.

Institutional Review Board Statement: Not applicable.

Informed Consent Statement: Not applicable.

Data Availability Statement: Not applicable.

Conflicts of Interest: The authors declare no conflict of interest.

References

1. Mou, Y.; Lian, Z.; Li, W.; Zhong, X.; Li, J.; He, Y.; Cao, J.; Eliaz, N. The effect of friction welding on the mechanical properties and corrosion fatigue resistance of titanium alloy drill pipe. *Fatigue Fract. Eng. Mater. Struct.* **2022**, *45*, 466–481. [[CrossRef](#)]
2. Jiang, L.; Feng, C.; Liu, H.Q.; Wang, L.; Han, L.H.; Feng, Y.R.; Li, F.P.; Lu, C.H.; Zhu, L.J.; Wang, H. Deformation Stability of a Low-Cost Titanium Alloy Used for Petroleum Drilling Pipe. In *Materials Science Forum*; Trans Tech Publications Ltd.: Wollerau, Switzerland, 2019; pp. 887–891.
3. Liu, Q.; Li, N.; Shen, Z.X.; Zhao, M.F.; Xie, J.F.; Zhu, G.C.; Xu, X.; Yin, C.X. Calculation model and experimental study of the collapse strength of titanium alloy tubing and casing. *Sci. Rep.* **2022**, *12*, 4526. [[CrossRef](#)] [[PubMed](#)]
4. Mla, C.; Ml, B.; Xtw, A.; Mcl, A.; Xl, A.; Zmr, A.; Ghc, A.; Zhz, C. Effect of tempering temperature at high temperature zone on sulfide stress cracking behavior for casing steel. *Eng. Fail. Anal.* **2019**, *105*, 227–236.
5. Wang, F.; Tan, X.; Wang, R.; Sun, M.; Wang, L.; Liu, J. High temperature and high pressure rheological properties of high-density water-based drilling fluids for deep wells. *Petrol. Sci.* **2012**, *9*, 354–362. [[CrossRef](#)]
6. Li, D.; Hui, S.X.; Ye, W.J.; Li, C.L. Microstructure and mechanical properties of a new high-strength and high-toughness titanium alloy. *Rare Met.* **2016**. [[CrossRef](#)]
7. Boehlert, C.J.; Tamirisakandala, S.; Curtin, W.A.; Miracle, D.B. Assessment of in situ TiB whisker tensile strength and optimization of TiB-reinforced titanium alloy design. *Scr. Mater.* **2009**, *61*, 245–248. [[CrossRef](#)]
8. Bodunrin, M.O.; Chown, L.H.; Merwe, J.; Alaneme, K.K.; Mphasha, N.P. Corrosion behavior of titanium alloys in acidic and saline media: Role of alloy design, passivation integrity, and electrolyte modification. *Corros. Rev.* **2020**, *38*, 25–48. [[CrossRef](#)]
9. Wegner, N.; Kotzem, D.; Wessarges, Y.; Emminghaus, N.; Hoff, C.; Tenkamp, J.; Overmeyer, L.; Walther, F. Corrosion and corrosion fatigue properties of additively manufactured magnesium alloy WE43 in comparison to titanium alloy Ti-6Al-4V in physiological environment. *Materials* **2019**, *12*, 2892. [[CrossRef](#)]
10. Kitashima, T.; Suresh, K.S.; Yamabe-Mitarai, Y. Effect of germanium and silicon additions on the mechanical properties of a near- α titanium alloy. *Mater. Sci. Eng. A* **2014**, *597*, 212–218. [[CrossRef](#)]
11. Chen, W. Preparation of Multiscale α Phase by Heat Treatments and Its Effect on Tensile Properties in Metastable β Titanium Alloy Sheet. *Metals* **2021**, *11*, 1708.
12. Long, W. Effect of Third-Stage Heat Treatments on Microstructure and Properties of Dual-Phase Titanium Alloy. *Materials* **2021**, *14*, 2776.
13. Gao, J.; Knowles, A.J.; Guan, D.; Rainforth, W.M. ω phase strengthened 1.2GPa metastable β titanium alloy with high ductility. *Scr. Mater.* **2018**, *162*, 77–81. [[CrossRef](#)]
14. Li, Y.; Liao, Z.; Zhang, W.; Wu, Z.; Zhou, C. Strength-Ductility Synergy in a Metastable β Titanium Alloy by Stress Induced Interfacial Twin Boundary ω Phase at Cryogenic Temperatures. *Materials* **2020**, *13*, 4732. [[CrossRef](#)] [[PubMed](#)]
15. Gao, J.; Nutter, J.; Liu, X.; Guan, D.; Rainforth, W.M. Segregation mediated heterogeneous structure in a metastable β titanium alloy with a superior combination of strength and ductility. *Sci. Rep.* **2018**, *8*, 7512. [[CrossRef](#)] [[PubMed](#)]
16. Chuan, W.; He, Y.; Wei, L.H. Substructure and texture evolution and flow behavior of TA15 titanium alloy compressed in the $\alpha + \beta$ two-phase field. *J. Mater. Process. Technol.* **2013**, *213*, 2033–2041. [[CrossRef](#)]
17. Dong, R.; Li, J.; Kou, H.; Fan, J.; Tang, B.; Sun, M. Precipitation behavior of α phase during aging treatment in a β -quenched Ti-7333. *Mater. Charact.* **2018**, *140*, 275–280. [[CrossRef](#)]
18. Sordi, V.L.; Ferrante, M.; Kawasaki, M.; Langdon, T.G. Microstructure and tensile strength of grade 2 titanium processed by equal-channel angular pressing and by rolling. *J. Mater. Sci.* **2012**, *47*, 7870–7876. [[CrossRef](#)]
19. Wang, L.; Lin, Z.; Wang, X.; Shi, Q.; Yin, W. Effect of Aging Treatment on Microstructure and Mechanical Properties of Ti27Nb2Ta3Zr β Titanium Alloy for Implant Applications. *Mater. Trans.* **2014**, *55*, 141–146. [[CrossRef](#)]
20. Thijs, L.; Verhaeghe, F.; Craeghs, T.; Humbeeck, J.V.; Kruth, J.P. A study of the microstructural evolution during selective laser melting of Ti-6Al-4V. *Acta Mater.* **2010**, *58*, 3303–3312. [[CrossRef](#)]
21. Stella, P.; Giovanetti, I.; Masi, G.; Leoni, M.; Molinari, A. Microstructure and microhardness of heat-treated Ti-6Al-2Sn-4Zr-6Mo alloy. *J. Alloy. Compd.* **2013**, *567*, 134–140. [[CrossRef](#)]
22. Reguly, C.K.A.J. Effect of plastic deformation on the toughness behaviour of radial friction welds in Ti-6Al-4V-0.1Ru titanium alloy. *Mater. Sci. Eng. A* **2006**, *417*, 49–55.
23. Du, Z.; Xiao, S.; Xu, L.; Jing, T.; Kong, F.; Chen, Y. Effect of heat treatment on microstructure and mechanical properties of a new β high strength titanium alloy. *Mater. Des.* **2014**, *55*, 183–190. [[CrossRef](#)]
24. Zhu, S.; Yang, H.; Guo, L.G.; Fan, X.G. Effect of cooling rate on microstructure evolution during α/β heat treatment of TA15 titanium alloy. *Mater. Charact.* **2012**, *70*, 101–110. [[CrossRef](#)]
25. Setti, S.G.; Rao, R.N. Tribological behaviour of near β titanium alloy as a function of $\alpha+\beta$ solution treatment temperature. *Mater. Des.* **2013**, *50*, 997–1004. [[CrossRef](#)]
26. Sang, W.L.; Kim, J.H.; Chan, H.P.; Hong, J.K.; Yeom, J.T. Alloy design of metastable $\alpha+\beta$ titanium alloy with high elastic admissible strain. *Mater. Sci. Eng. A* **2021**, *802*, 140621.
27. Wang, G.; Chen, Z.; Li, J.; Liu, J.; Yang, R. Microstructure and Mechanical Properties of Electron Beam Welded Titanium Alloy Ti-6246. *Acta Metall. Sin.* **2016**, *34*, 570–576. [[CrossRef](#)]
28. Hurlley, P.J.; Whittaker, M.T.; Webster, P.; Evans, W.J. A methodology for predicting creep/fatigue crack growth rates in Ti 6246. *Int. J. Fatigue* **2007**, *29*, 1702–1710. [[CrossRef](#)]

29. Whittaker, M.T.; Evans, W.J.; Hurley, P.J.; Flynn, D. Prediction of notched specimen behaviour at ambient and high temperatures in Ti6246. *Int. J. Fatigue* **2007**, *29*, 1716–1725. [[CrossRef](#)]
30. Zhang, Z.Q.; Dong, L.M.; Yang, Y.; Guan, S.X.; Liu, Y.Y.; Yang, R. Microstructure refinement of a dual phase titanium alloy by severe room temperature compression. *Trans. Nonferrous Met. Soc. China* **2012**, *22*, 2604–2608. [[CrossRef](#)]
31. Chen, Y.; Yang, C.; Fan, C.; Zhuo, Y.; Chen, C. Grain refinement of additive manufactured Ti-6.5Al-3.5Mo-1.5Zr-0.3Si titanium alloy by the addition of La₂O₃. *Mater. Lett.* **2020**, *275*, 128170. [[CrossRef](#)]
32. Ding, C.; Liu, C.; Zhang, L.; Deng, Y.; Liu, H.; Wu, D.; Liu, L. Microstructure and tensile properties of a cost-affordable and ultrahigh-strength metastable β titanium alloy with a composition of Ti-6Al-1Mo-1Fe-6.9Cr. *J. Alloy. Compd.* **2022**, *901*, 163476. [[CrossRef](#)]
33. Liu, F.; Chen, Y.; He, C.; Li, L.; Liu, Y. Tensile and very high cycle fatigue behaviors of a compressor blade titanium alloy at room and high temperatures. *Mater. Sci. Eng. A* **2021**, *811*, 141049. [[CrossRef](#)]
34. Wei, W.; Feng, Y.; Han, L.; Zhang, Q.; Zhang, J. Cyclic hardening and dynamic strain aging during low-cycle fatigue of Cr-Mo tempered martensitic steel at elevated temperatures. *Mater. Sci. Eng. A* **2018**, *734*, 20–26. [[CrossRef](#)]
35. Lü, Z.; Zhang, C.J.; Du, Z.X.; Han, J.C.; Zhang, S.Z.; Yang, F.; Chen, Y.Y. Relationship between microstructure and tensile properties on a near- β titanium alloy after multidirectional forging and heat treatment. *Rare Met.* **2019**, *38*, 7. [[CrossRef](#)]